An efficient approach for eigenmode analysis of transient distributive mixing by the mapping method

An efficient approach for eigenmode analysis of transient distributive mixing by the mapping method

O. Gorodetskyi, M. F. M. Speetjens, and P. D. Anderson
Department of Mechanical Engineering, Eindhoven University of Technology, PO box 513, 5600 MB Eindhoven, The Netherlands

(Received 4 July 2011; accepted 17 November 2011; published online 9 May 2012)

The mapping method is an efficient tool to investigate distributive mixing induced by periodic flows. Computed only once, the mapping matrix can be applied a number of times to determine the distribution of concentration inside the flow domain. Spectral analysis of the mapping matrix reveals detailed properties of the distributive mixing as all relevant information is stored in its eigenmodes. Any vector that describes a distribution of concentration can be expanded in the complete system of linearly independent eigenvectors of the mapping matrix. The rapid decay of the contribution of each mode in the eigenmode decomposition allows for a truncation of the eigenmode expansion from the whole spectrum to only the dominant eigenmodes (characterized by a decay rate significantly lower than the duration of the mixing process). This truncated decomposition adequately represents the distribution of concentration inside the flow domain already after a low number of periods, because contributions of all non-dominant eigenmodes rapidly become insignificant. The truncation is determined independently of the initial distribution of concentration and based on the decay rates of the eigenmodes, which are inversely proportional to the corresponding eigenvalues. Only modes with eigenvalues above a certain threshold are retained. The key advantage of the proposed compact eigenmode representation of the mapping method is that it includes practically relevant transient states and not just the asymptotic one. As such the method enables an eigenmode analysis of realistic problems yet with a substantial reduction in computational effort compared to the conventional approach.
 [http://dx.doi.org/10.1063/1.4712133]

I. INTRODUCTION

Fluid mixing is central to many natural and engineered processes at both large and small scales. The prediction and analysis of mixing and transport patterns is not only relevant in industrial mixers and microfluidic systems, but also in geophysical, oceanographic, and atmospheric flows. Further examples include population genetics, distribution of nutrients, oil spills and the prediction of the weather.[1–6] Spectral analysis has become popular for the investigation of scalar transport in such flows, as the governing advection-diffusion equation is linear and thus amenable to characterization in terms of the eigenvalues and eigenvectors of the evolution operator.[7] Analysis of its spectral structure has been performed in Cerbelli *et al.*[8] and revealed an exponential decay of the scalar field towards a homogeneous asymptotic state. Here the spatial structure of the decaying scalar field rapidly becomes dominated by the slowest-decaying eigenmode, termed "strange eigenmode" by Pierrehumbert,[9] to which many studies have been dedicated to date.[10–16] Strange eigenmodes are in literature commonly associated with chaotic advection. In the present context we adopt the more generic term "dominant eigenmodes" for slowest-decaying eigenmodes. Such modes can during transient mixing, namely, be distinguished for both islands and chaotic seas.

In the present work only advective transport of material is considered and described by means of the mapping method. Eigenmode decompositions of the mapping matrix reveal important insight into the generic transport properties of mixing flows. Singh *et al.*[17] presented a first analysis of the eigenmode decomposition of the mapping matrix and connected its spectral properties with mixing

characteristic and coherent structures in the Lagrangian flow structure (i.e., islands and chaotic regions). For mixing simulations in realistic industrial devices, the mapping matrix is sparse and of a huge size, which makes calculation of the whole spectrum computationally very expensive and in many cases even impossible. Thus an alternative, more efficient way is required to perform eigenmode analyses in such configurations.

In practice, mixing processes are generally determined by the transient evolution of concentration distributions, meaning that asymptotic mixing states, the focus of typical eigenmode analyses, are in general less relevant in such applications. For example, in microfluidic mixers usually mixing takes place within a limited span of no more than ten spatial periods. Hence, an efficient method for eigenmode analysis of realistic mixing flows must be developed specifically for transient mixing. Essential to transient mixing is that its evolution depends not only on the dominant eigenmodes, but also on the specific contribution of eigenmodes with decay rate significantly lower than the duration of the mixing process ("transient eigenmodes"). The relevance of multiple eigenmodes during the transient means that it, in contrast with the dependence of the asymptotic state solely on the dominant eigenmode, depends essentially on the initial state. Thus, determining said specific contribution is essential to eigenmode analyses of transient mixing. However, in the standard mapping method, this, first, requires a full eigenmode decomposition of the mapping matrix and, second, a full evaluation of the expansion coefficients of all eigenmodes for given initial conditions. These are generally computationally very expensive manipulations and therefore not an option for typical practical mixing studies.

The present study offers a way for efficient eigenmode analysis of transient mixing. The basic course of action is as follows. First, systematic isolation of the compact eigenmode basis (defined by the set of transient eigenmodes including the dominant eigenmode) that contains all "essential" information. Second, efficient evaluation of the specific contribution of the relevant eigenmodes based on orthogonalization of the compact basis. This admits a case-specific eigenmode analysis and isolation of possible modes within the compact basis that dominate the transient in a similar way as the dominant eigenmode at some point overrules all other modes. Such "dominant transient eigenmodes," the excitation of which depends essentially on the initial state, may play a role of equal – if not higher – significance than the dominant eigenmode in realistic mixing processes. This may deepen understanding of mixing processes and may also facilitate further reduction of the compact eigenmode basis for the benefit of computational efficiency.

The paper is organized as follows. Section II briefly reviews the mapping method and eigenmode decomposition of the mapping matrix including an illustrative example. Section III introduces the compact mapping method, based on the truncated eigenmode decomposition of the mapping matrix, and the orthogonalization procedure for efficient evaluation of the expansion coefficients for the compact basis in case of arbitrary initial conditions. The compact mapping method is demonstrated and its performance evaluated by way of comparison with the conventional mapping method in Sec. IV. Conclusions are drawn in Sec. V.

II. THE MAPPING METHOD FOR DISTRIBUTIVE MIXING

A. The mapping matrix and its construction

The mapping method was originally proposed by Spencer and Wiley[18] and has proven its worth for the simulation and analysis of laminar mixing.[19–23] This ansatz describes mixing by the redistribution of material over a grid of discrete cells via the so-called mapping matrix, the entries of which represent the fractions of material exchanged between cells. A computationally efficient way to determine these fractions is by representation of the continuous material within cells by discrete markers, as shown schematically in Figure 1.[24] The domain is subdivided into N cells that each hold M_j markers, which are advected by the flow during the time interval $t_0 \leq t \leq t_0 + \triangle t$. Entries of the mapping matrix then are defined by

$$\mathbf{\Phi}_{ij} = \frac{M_{ij}}{M_j}, \tag{1}$$

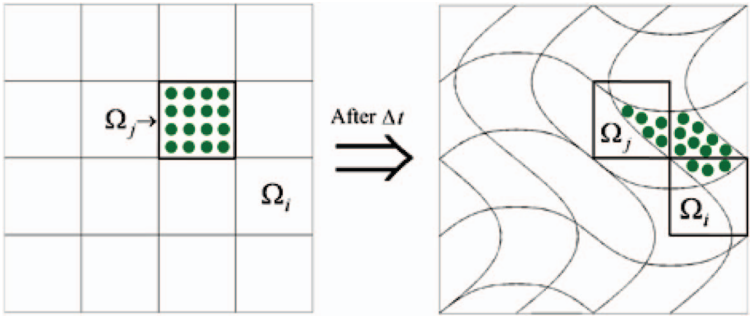

FIG. 1. Illustration of the computation of the entries $\boldsymbol{\Phi}_{ij}$ of the mapping matrix $\boldsymbol{\Phi}$. The cell Ω_j at $t = t_0$ is covered with a number of markers that are tracked during flow in Δt to arrive at the final cross section $t = t_0 + \Delta t$. The ratio of the number of markers received by the recipient cell Ω_i to the initial number of markers in Ω_j is determined. In this case $\boldsymbol{\Phi}_{ij} = \frac{3}{16}$.

with M_{ij} the number of markers – and $\boldsymbol{\Phi}_{ij}$ the corresponding fraction – fraction of the M_j markers in donor cell Ω_j at $t = t_0$ ending up in the recipient cell Ω_i at $t = t_0 + \Delta t$. The constructed mapping matrix allows to compute the redistribution of any arbitrary initial concentration $\boldsymbol{C}_0 \in R^{N\times 1}$ of material over the N cells during the above time interval via

$$\boldsymbol{C}_1 = \boldsymbol{\Phi}\boldsymbol{C}_0, \tag{2}$$

with $\boldsymbol{C}_1 \in R^{N\times 1}$ the new concentration.

The present study is restricted to time-periodic flows $\boldsymbol{u}(\boldsymbol{x}, t) = \boldsymbol{u}(\boldsymbol{x}, t + T)$, with period time T. Constructing the mapping matrix for time interval $0 \le t \le T$ then admits computation of period-wise redistribution of material by repetitive mapping following

$$\boldsymbol{C}_n = (\underbrace{\boldsymbol{\Phi}(\boldsymbol{\Phi}(...(\boldsymbol{\Phi}}_{\text{n times}}\boldsymbol{C}_0)...))) = \boldsymbol{\Phi}^n\boldsymbol{C}_0, \tag{3}$$

with $\boldsymbol{C}_n$ the resulting concentration after n periods. Details of the method, with validation and comparisons with other methods, are found in Kruijt *et al.*[19] and Singh *et al.*[24]

B. Eigenmode decomposition of the mapping matrix

The concentration according to Eq. (3) admits the eigenmode decomposition

$$\boldsymbol{C}_n = \sum_{k=1}^{N} C_k^0 \lambda_k^n \boldsymbol{v}_k, \tag{4}$$

with $\{\lambda_k, \boldsymbol{v}_k\}$ the corresponding eigenvalue-eigenvector pairs of the mapping matrix $\boldsymbol{\Phi}$ and C_k^0 the expansion coefficients.[17] These eigenmodes constitute the "fingerprint" of the mapping matrix and contain all information about the transport properties. Both the mapping matrix and the concentration vectors are real. This has a number of essential ramifications. First, eigenmodes are either real or emerge as complex conjugate pairs $\{\lambda_k, \lambda_{k+1}\} = \{\lambda_k, \lambda_k^*\}$ and $\{\boldsymbol{v}_k, \boldsymbol{v}_{k+1}\} = \{\boldsymbol{v}_k, \boldsymbol{v}_k^*\}$. Second, expansion coefficients associated with such pairs must also form complex-conjugate pairs: $\{C_k^0, C_{k+1}^0\} = \{C_k^0, C_k^{0,*}\}$. Thus, the initial concentration can be expressed as

$$\boldsymbol{C}_0 = \cdots + C_p^0 \boldsymbol{v}_p + \cdots + 2\mathrm{Re}(C_k^0)\mathrm{Re}(\boldsymbol{v}_k) - 2\mathrm{Im}(C_k^0)\mathrm{Im}(\boldsymbol{v}_k) + \cdots \tag{5}$$

with the leading term representing real eigenmodes and the remaining terms representing complex-conjugate pairs. The corresponding concentration after n periods according to Eq. (4) thus in effect

reads

$$\boldsymbol{C}_n = \cdots + C_p^0 \lambda_k^n \boldsymbol{v}_p + \cdots + 2\mathrm{Re}(C_k^0)|\lambda_k^n| \begin{bmatrix} V_{k,0}\cos(\alpha_{k,0}+n\phi_k) \\ \vdots \\ V_{k,N}\cos(\alpha_{k,N}+n\phi_k) \end{bmatrix}$$

$$-2\mathrm{Im}(C_k^0)|\lambda_k^n| \begin{bmatrix} V_{k,0}\sin(\alpha_{k,0}+n\phi_k) \\ \vdots \\ V_{k,N}\sin(\alpha_{k,N}+n\phi_k) \end{bmatrix} + \ldots, \tag{6}$$

where $V_{k,i} = |\boldsymbol{v}_{k,i}|$, $\alpha_{k,i} = \arg(\boldsymbol{v}_{k,i})$, $\phi_k = \arg(\lambda_k)$.

The eigenvalues are bounded by $|\lambda_k| \leq 1$, meaning that eigenmodes either decay exponentially in time ($|\lambda_k| < 1$) or persist indefinitely ($|\lambda_1| = 1$). The persistent modes determine the asymptotic state $\boldsymbol{C}_\infty := \lim_{n\to\infty} \boldsymbol{C}_n$; the decaying modes determine the progression towards this state. This progression, after a short-lived initial stage, rapidly becomes dominated by the slowest-decaying eigenmode(s), that is, the (cluster of) eigenmode(s) with eigenvalue(s) closest to the unit circle in the complex plane spanned by (Re(λ), Im(λ)). These modes correspond with $\max|\lambda_k| = \lambda_{\mathrm{dom}} < 1$ and are, consistent with the nomenclature introduced in Sec. I, denoted "dominant eigenmodes" hereafter. The mapping matrix always possesses a trivial persistent eigenmode with $\lambda_1 = 1$ and $\boldsymbol{v}_k = \gamma\mathbf{1}$, where $\mathbf{1}$ is the unit vector and γ is an arbitrary constant, due to mass conservation. Absence of other persistent modes implies a homogeneous asymptotic state and signifies chaotic mixing. The presence of such modes implies persistent inhomogeneities and, inherently, incomplete mixing.[17] The above properties are based on the generic conjectures advanced in Singh *et al.*[17] We must stress that proof of these conjectures is still outstanding. However, numerical evidence so far fully supports these conjectures.

Important to note is that purely advective mixing strictly confines the eigenvalue spectrum of the transport operator to the unit circle.[25,26] This implies a unitary mapping matrix. However, the mapping matrix possesses this property only in the hypothetical case of infinite spatial resolution. Actual mapping matrices are constructed from a finite number of cells and, in consequence, suffer from numerical diffusion. This, similar to the effect of molecular diffusion in advective-diffusive transport, manifests itself in local smearing-out of spatial features in the mixing pattern and causes the eigenvalue spectrum to fall within the unit circle.[17] The eigenmodes of the actual mapping matrix nonetheless are physically meaningful in that they are locally averaged representations of the eigenmodes of the ideal unitary mapping matrix. The smearing-out becomes more profound the finer the spatial features and shifts the eigenvalues of corresponding eigenmodes further within the unit circle.

C. An illustrative example

The present study adopts the well-known time-periodic sine flow (TPSF) as prototype mixing flow.[8,12,27,28] It consists of periodically reoriented steady sinusoidal flows inside the bi-periodic square $\Omega = (0, 1) \times (0, 1)$ and is given by

$$(u_x, u_y) = [\sin(2\pi y), 0] \quad \text{for } 0 \leq t \leq \frac{T}{2}, \quad (u_x, u_y) = [0, \sin(2\pi x)] \quad \text{for } \frac{T}{2} \leq t \leq T, \tag{7}$$

with T the period time. The TPSF admits an analytical expression for the period-wise mapping of markers, reading

$$x_i = \mathrm{mod}[\{x_{i-1} + 0.5T\sin(2\pi y_{i-1})\}, 1], \quad y_i = \mathrm{mod}[\{y_{i-1} + 0.5T\sin(2\pi x_i)\}, 1], \tag{8}$$

which enables an accurate and efficient computation of the associated mapping matrix.

The flow structure – and corresponding mixing properties – can be made visible by Poincaré sections.[29] This is demonstrated in Figure 2 for the three stirring protocols corresponding with $T = 0.56$, $T = 1.12$, and $T = 1.6$, exposing the characteristic flow structure of 2D mixing flows:

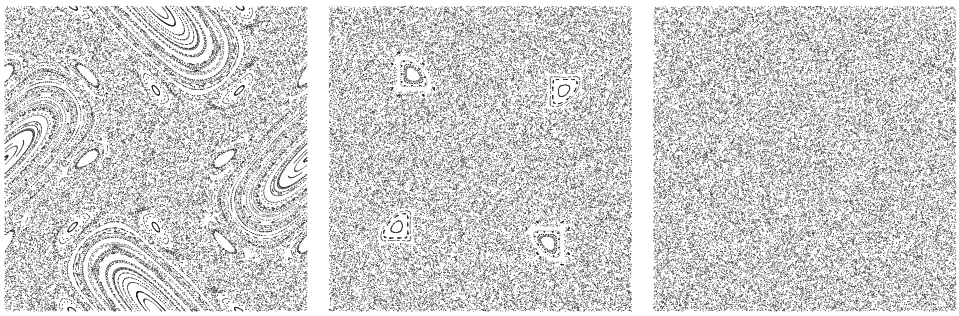

FIG. 2. Poincaré-sections of the TPSF for different periods T.

islands and chaotic seas. The progression with growing T reveals a gradual diminution of islands in favor of a chaotic sea until a state of global chaos sets in beyond a certain T.

The Poincaré sections visualize the asymptotic state of the system and their structure, in consequence, is intimately related to the persistent and dominant eigenmodes of the mapping matrix.[8,17] Figures 3(a) and 3(b) show typical persistent modes for cases $T = 0.56$ and $T = 1.12$, respectively, and reveal that their structure coincides with the islands in the associated Poincaré sections (Figure 2). Figure 3(c) gives the isolated dominant eigenmode for $T = 1.6$ with corresponding eigenvalue $\lambda_{\text{dom}} = 0.58$. Non-trivial persistent modes are absent here, consistent with the state of global chaos. The structure of the isolated dominant eigenmode defines the asymptotic mixing pattern within the chaotic sea. Figure 3(d) gives the dominant eigenmode in the chaotic sea for $T = 0.56$ with corresponding eigenvalue $\lambda_{\text{dom}} = 0.91$.

Key advantages of the eigenmode analysis over Poincaré sectioning are, first, that this ansatz affords deeper (quantitative) insight into the mixing properties and, second, that it admits investigation of the transient via which the system approaches the asymptotic state. Downside is that this is

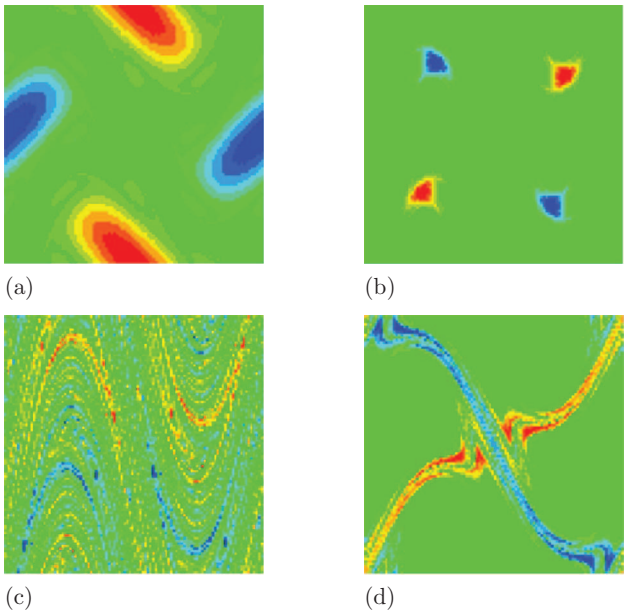

FIG. 3. Second-dominant eigenvectors for: (a) $T = 0.56$; (b) $T = 1.12$; (c) $T = 1.6$; (d) dominant eigenmode chaotic sea for $T = 0.56$. Second-dominant eigenmodes are real for any T. Background shade (green) corresponds to zero values of the eigenvector.

computationally more intensive. An efficient way to carry out such an eigenmode analysis by way of the mapping matrix is elaborated hereafter.

III. COMPACT MAPPING METHOD

A. Reduced eigenmode representation of the mapping method

An important consequence of the exponential decline of the decaying eigenmodes is that the set of modes that significantly contributes to the eigenmode decomposition (4) – and thereby to the evolution of the concentration field – decreases rapidly with increasing number of periods n. This implies that Eq. (4), upon arranging the eigenmodes by descending order of eigenvalue magnitude, i.e., $|\lambda_N| \leq \cdots \leq |\lambda_1| \leq 1$, effectively reduces to the compact form,

$$\boldsymbol{C}_n = \sum_{k=1}^{M} C_k^0 \lambda_k^n \boldsymbol{v}_k + \epsilon_n, \quad \epsilon_n \sim \mathcal{O}(|\lambda_{M+1}|^n), \tag{9}$$

with $k \leq M$ the relevant eigenmodes upon permitting a certain truncation error ϵ_n. Its validity is demonstrated in Sec. IV. Practical mixing analyses typically admit $M \ll N$ at an only marginal loss of accuracy after already a limited number of periods n. Thus, the compact representation paves the way to eigenmode analyses of the – in practice highly relevant – transient states during mixing by including only subspectrum $k \leq M$ and not the full spectrum $k \leq N$; isolation of the latter is extremely expensive and not an option in most cases. This *modus operandi* in essence is a generalization of the concept of dominant and persistent eigenmode(s) for the asymptotic mixing state (Sec. II B) in that transient mixing, within a controllable error $\mathcal{O}(\epsilon_n)$, is described by its "dominant eigenspace" $k \leq M$. This eigenspace naturally incorporates the eigenmodes of the asymptotic state and the retained eigenmodes of the transient (termed "transient eigenmodes" hereafter). Fundamental difference with asymptotic analyses is that during transients the interplay of eigenmodes in this eigenspace is key to the overall system evolution. This depends essentially on the case-specific spectrum C_k^0 ($k \leq M$) of the initial state $\boldsymbol{C}_0$. Efficient evaluation of this spectrum is discussed in Sec. III B.

Introducing ϵ as the, to be specified, tolerance via the truncation error in Eq. (9) advances

$$|\lambda_{M+1}|^{n_\epsilon} = \epsilon \tag{10}$$

as an implicit relation between the cut-off M (via eigenvalue λ_{M+1}) and the number of periods n_ϵ after which the compact representation (9) becomes reliable. This preset tolerance ϵ thus enables the determination of n_ϵ for given M or *vice versa.* The present study adopts the former option, which can be done without loss of generality, and leads to the practical estimators

$$n_\epsilon = \frac{\ln \epsilon}{\ln |\lambda_{M+1}|}, \quad n_\infty = \frac{\ln \epsilon}{\ln |\lambda_{\mathrm{dom}}|}, \quad n' \equiv 1 - \frac{n_\epsilon}{n_\infty} = \frac{\ln(|\lambda_{M+1}|/|\lambda_{\mathrm{dom}}|)}{\ln |\lambda_{M+1}|}, \tag{11}$$

with n_ϵ as before, n_∞ signifying the onset of the asymptotic state and n' the relative part of the transient that can be reliably captured by the compact representation (9). Note that the estimator n' solely depends on the cut-off M.

B. Modal decomposition of the initial state

Isolation of the case-specific spectrum C_k^0 ($k \leq M$) for a given initial state $\boldsymbol{C}_0$ follows from the compact representation (9). Reformulate to this end the latter as

$$\widetilde{\boldsymbol{C}}_0 = \sum_{k=1}^{M} \widetilde{C}_k^0 \boldsymbol{v}_k + \epsilon_n, \quad \epsilon_n \sim \mathcal{O}(\epsilon), \quad \widetilde{\boldsymbol{C}}_0 \equiv \boldsymbol{\Phi}^n \boldsymbol{C}_0, \quad \widetilde{C}_k^0 \equiv C_k^0 \lambda_k^n, \tag{12}$$

with $\widetilde{C}_k^0$ expansion coefficients of the scalar field (at period n) in terms of the compact eigenvector basis and tolerance ϵ following Eq. (10), meaning that the truncation error ϵ_n can be made arbitrarily

small by a sufficiently high n. This admits a very precise approximation of the spectrum C_k^0. Note that n employed here is unrelated to that used in demarcation of the dominant eigenspace of the transient. The expansion coefficients $\widetilde{C}_k^0$ can be efficiently evaluated by way of a similarity transform of the compact eigenvector basis $(\boldsymbol{v}_1, \ldots, \boldsymbol{v}_M)$ into an equivalent orthogonal basis $(\boldsymbol{u}_1, \ldots, \boldsymbol{u}_M)$.

Orthogonalization requires the vectors $(\boldsymbol{v}_1, \ldots, \boldsymbol{v}_M)$ to be real and linearly independent.[30–32] Relation (6) implies that the eigenvectors of the mapping matrix can be readily transformed in an equivalent basis consisting of real vectors $(\boldsymbol{v}_1, \ldots, \boldsymbol{v}_M)$ by expressing complex-conjugate pairs of complex vectors, if present, in terms of their real and imaginary parts. Moreover, provided sufficient spatial resolution, vectors $\boldsymbol{v}_i$ represent unique physical eigenmodes and thus are linearly independent. Hence, the present system can be made to fulfill the above conditions and thus admits orthogonalization.

Orthogonalization aims at transformation of the present system into an equivalent system $(\boldsymbol{u}_1, ..., \boldsymbol{u}_M)$ subject to the orthogonality condition

$$\boldsymbol{u}_i \cdot \boldsymbol{u}_j = 0 \quad \text{if } i \neq j. \tag{13}$$

This embarks on expanding each vector $\boldsymbol{u}_i$ as a linear combination of vectors $\boldsymbol{v}_j$ according to

$$\begin{aligned}
\boldsymbol{u}_1 &= \boldsymbol{v}_1, \\
\boldsymbol{u}_2 &= \boldsymbol{v}_2 + a_{11}\boldsymbol{v}_1, \\
\boldsymbol{u}_3 &= \boldsymbol{v}_3 + a_{21}\boldsymbol{v}_1 + a_{22}\boldsymbol{v}_2, \\
&\vdots \\
\boldsymbol{u}_M &= \boldsymbol{v}_M + a_{(M-1)1}\boldsymbol{v}_1 + \cdots + a_{(M-1)(M-1)}\boldsymbol{v}_{M-1},
\end{aligned} \tag{14}$$

where expansion coefficients a_{ij} are determined by condition (13).[32] Condition $\boldsymbol{u}_1 \cdot \boldsymbol{u}_2 = 0$ gives $a_{11} = -\frac{\boldsymbol{v}_1 \cdot \boldsymbol{v}_2}{\boldsymbol{v}_1 \cdot \boldsymbol{v}_1}$; coefficients a_{12} and a_{22} can subsequently be obtained from $\boldsymbol{u}_3 \cdot \boldsymbol{u}_1 = 0$ and $\boldsymbol{u}_3 \cdot \boldsymbol{u}_2 = 0$. The remaining coefficients follow in a similar way from continuing this procedure top down towards $a_{(M-1)(M-1)}$.

The orthogonality condition (13) can be recast as

$$\boldsymbol{u}_i \cdot \boldsymbol{v}_j = 0, \quad \text{if } j < i, \tag{15}$$

and in this form facilitates evaluation of the sought-after expansion coefficients $\widetilde{C}_k^0$. The inner product of expansion (12) with $\boldsymbol{u}_M$ yields

$$\widetilde{\boldsymbol{C}}_0 \cdot \boldsymbol{u}_M = \sum_{k=1}^{M} \widetilde{C}_k^0 \boldsymbol{v}_k \cdot \boldsymbol{u}_M = \widetilde{C}_M^0 \boldsymbol{v}_M \cdot \boldsymbol{u}_M \quad \Rightarrow \quad \widetilde{C}_M^0 = \frac{\widetilde{\boldsymbol{C}}_0 \cdot \boldsymbol{u}_M}{\boldsymbol{v}_M \cdot \boldsymbol{u}_M}, \tag{16}$$

by virtue of Eq. (15). Subsequently taking the inner product with $\boldsymbol{u}_{M-1}$ gives

$$\widetilde{\boldsymbol{C}}_0 \cdot \boldsymbol{u}_{M-1} = \widetilde{C}_{M-1}^0 \boldsymbol{v}_{M-1} \cdot \boldsymbol{u}_{M-1} + \widetilde{C}_M^0 \boldsymbol{v}_M \cdot \boldsymbol{u}_{M-1} \tag{17}$$

as expression for evaluation of $\widetilde{C}_{M-1}^0$. The remaining expansion coefficients $(\widetilde{C}_{M-2}^0, \ldots, \widetilde{C}_1^0)$ follow from repeating this procedure. Back transformation via Eq. (12) yields spectrum C_k^0.

IV. ANALYSIS OF THE COMPACT MAPPING METHOD

A. Generic properties of the dominant eigenspace

The properties of the dominant eigenspace are demonstrated by way of the TPSF flow for $T = 0.56$ and $T = 1.6$. The former is characterized by the existence of elliptic islands and thus constitutes a poor-mixing flow; the latter exhibits global chaos and thus corresponds with a good-mixing flow (Figure 2). Here the compact basis is defined by setting the cut-off at $M = 500$ for

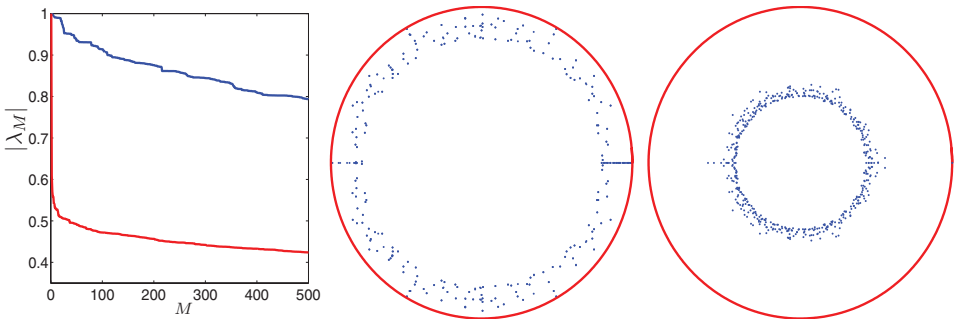

FIG. 4. Eigenvalue spectrum in the unit circle for the first 500 dominant eigenmodes of the mapping matrix associated with the TPSF in cases : (b) $T = 0.56$; (c) $T = 1.6$. Panel (a) corresponds to $|\lambda_M|$ for $T = 0.56$ - higher line (blue) and $T = 1.6$ - lower line (red line).

a full spectrum encompassing $N = 10\,000$ modes (mapping grid consisting of 100×100 cells), which is a significant reduction to a compact eigenspace that is 5% of the size of the full eigenspace. The corresponding spectra within this range are given in Figure 4 and expose an expressive difference between cases $T = 0.56$ and $T = 1.6$. Eigenvalues associated with non-trivial eigenmodes of the poor-mixing case $T = 0.56$ gradually decline from unity with increasing mode number; eigenvalues of the good-mixing case $T = 1.6$, in stark contrast, instantaneously drop off to $\lambda_{\text{dom}} = 0.58$ prior to such decay. This is a direct consequence of the absence of non-trivial persistent eigenmodes in the chaotic case (Sec. II B). Hence, the (compact) eigenvalue spectra close to the unit circle signifies poor mixing. Conversely, spectra well within the unit circle reflect the absence of non-trivial persistent modes and, inherently, (at least in asymptotic sense) good mixing. Concluded is that the compact eigenvalue spectra provides a first insight into the qualitative mixing properties.

The primary motivation for the compact mapping method is facilitating eigenmode analysis of *transient* mixing at a reasonable computational cost. Estimators (11) enable the determination of the range of the transient that can be reliably captured this way. The present cut-off at $M = 500$ yields $|\lambda_{M+1}| = 0.79$ and $|\lambda_{M+1}| = 0.31$ for $T = 0.56$ and $T = 1.6$, respectively, and dominant eigenvalues λ_{dom} are according to Sec. II C. This gives $n' = 0.5844$ ($T = 0.56$) and $n' = 0.5362$ ($T = 1.6$), meaning that the compact method, after reduction of the eigenspace to only 5% of its original size, nonetheless reliably represents about 50%–60% of the transient for any given tolerance ϵ. This reflects the strength of the compact mapping method. The actual range $n \in [n_\epsilon, n_\infty]$ of the transient depends on the tolerance ϵ. For $\epsilon = 10^{-8}$ this gives $n \in [82, 196]$ ($T = 0.56$) and $n \in [16, 134]$ ($T = 1.6$). However, typical engineering applications are restricted to much lower precision, say $\epsilon = 0.1(10^{-2})$, leading to $n \in [10, 24]([21, 49])$ and $n \in [2, 5]([4, 9])$ for $T = 0.56$ and $T = 1.6$, respectively. This reveals that, in particular for the chaotic flow, the earlier stages of the transient mixing become within the reach of the compact method. Increasing the cut-off M substantially extends this reach. In addition, the analysis in Sec. IV B exposes this assessment as rather conservative in the sense that mixing patterns are predicted better than suggested here.

The dominant eigenspace is spanned by the dominant/persistent eigenmodes of the asymptotic state, as shown in Sec. II C, and the transient eigenmodes (Sec. III A). Figure 5 shows typical transient eigenmodes of the poor-mixing case $T = 0.56$ and reveals that their spatial structure is consistent with that of the Poincaré section (Figure 2). This has the important implication that transient eigenmodes invariably respect the transport barriers demarcated by the flow topology. Their zones of influence may vary greatly, however. The transient mode in panel (a) is non-zero only within the island cores and thus contributes solely to the evolution within these regions; the mode in panel (b) acts in both the encircling island chains and associated chaotic bands. The

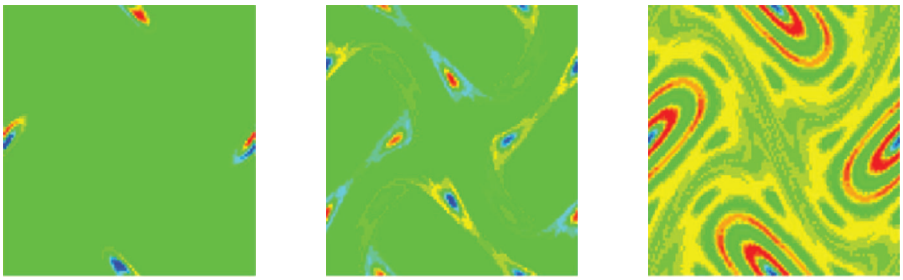

(a) (b) (c)

FIG. 5. Typical transient eigenmodes for $T = 0.56$.

transient mode in panel (c) covers the entire island region and even includes non-zero, albeit very weak, non-zero regions in the chaotic sea. Previous studies found that the decay rate in the chaotic sea is consistent with its dominant eigenmode.[17] Here this implies that transient modes covering both islands and chaotic sea must decay faster than this dominant mode. Further investigation of this issue is beyond the present scope. Figure 6 shows typical transient eigenmodes of the good-mixing case $T = 1.6$, which all are of similar structure as the corresponding dominant eigenmode (Figure 3(d)). Hence, the same spatial consistency as in the poor-mixing case exists between eigenmodes.

B. Performance of the compact mapping method

The performance of the compact mapping method for prediction and analysis of transient mixing is investigated hereafter for the above poor-mixing ($T = 0.56$) and good-mixing ($T = 1.6$) flows at $N = 10\,000$ and various cut-offs M. The initial state consists of a binary concentration distribution with $\boldsymbol{C} = 0$ and $\boldsymbol{C} = 1$ for $0 \leq y \leq 1/2$ and $1/2 < y \leq 1$, respectively, and its corresponding case-specific spectrum C_k^0 ($k \leq M$) is computed via the procedure outlined in Sec. III B using tolerance $\epsilon = 10^{-11}$ in Eq. (12). Estimators (11) define the lower bound n_ϵ for the number of periods n required to attain this precision at given cut-off M. The poor-mixing case employs $M = [500, 1000, 2000]$, yielding $n_\epsilon = [75, 55, 45]$; the good-mixing case employs $M = [100, 500, 1000]$, resulting in $n_\epsilon = [25, 18, 15]$. Compliance with condition $\epsilon_n \leq \epsilon$ has been verified numerically; this (i) ensures a very accurate approximation of the spectrum C_k^0 ($k \leq M$) and (ii) provides a first validation of estimators (11). Modal analysis of spectrum C_k^0 is considered in Sec. IV C. Note that cut-offs M are smaller for the good-mixing case on grounds of the steeper decline of the eigenvalue spectrum (Figure 4).

Figure 7 gives the evolution of the initial state over the first 10 periods of the transient for the poor-mixing case $T = 0.56$ according to the full method (panel a) in comparison to the compact method for $M/N = 20\%$ (panel b), $M/N = 10\%$ (panel c), $M/N = 5\%$ (panel d). This exposes an overall

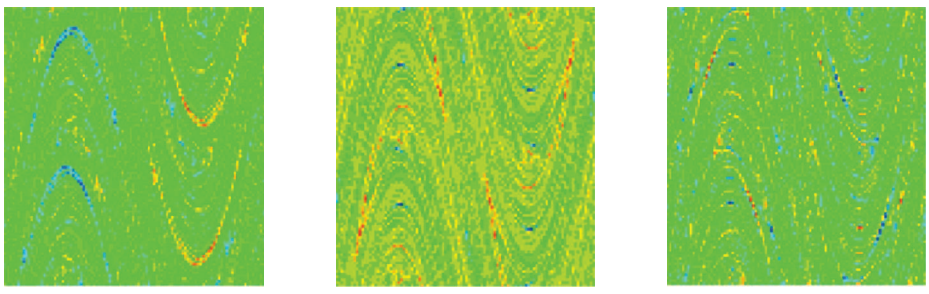

(a) (b) (c)

FIG. 6. Typical transient eigenmodes for $T = 1.6$.

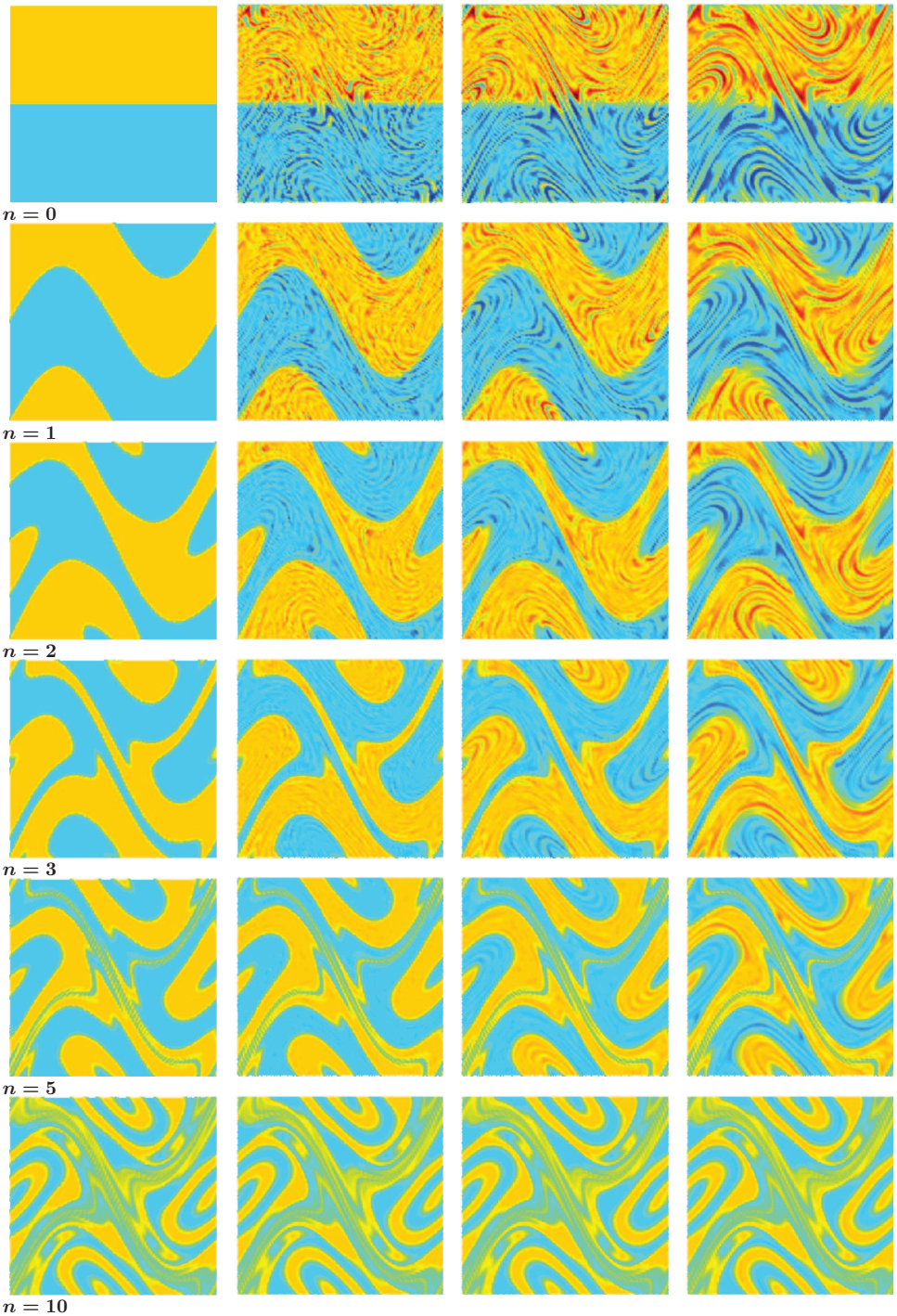

FIG. 7. Evolution for poor-mixing case $T = 0.56$: (a) full mapping method; (b)–(d) compact method for M/N as indicated. Color coding is identical throughout evolution; the color blue/red indicates $C = 0/C = 1$.

outstanding qualitative agreement between full and compact methods in that mixing patterns are accurately demarcated by the latter throughout the entire progression. Notable qualitative departures are restricted to localized artificial "ripples" in the concentration field that emerge during the first two periods and become more pronounced with lower M/N. The "ripples" observed in Figure 7

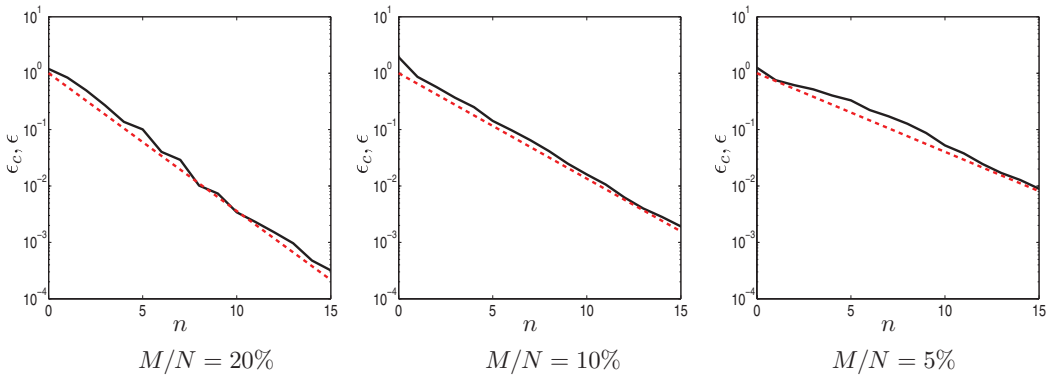

FIG. 8. Departure $\epsilon_c = |\boldsymbol{C}_n - \widetilde{\boldsymbol{C}}_n|$ (solid black line) and its prediction $\epsilon = |\lambda_{M+1}|^n$ dashed line (red) according to Eq. (10) for the poor-mixing case $T = 0.56$ and M/N as indicated. Bright and dark areas indicate region of applicability compact method on basis of n following Eq. (11) for $\epsilon = 10\%$ and $\epsilon = 1\%$, respectively.

originate from the approximation of the initial state. Remarkable is that, despite these "ripples," overall concentration levels within the patterns are still comparable. The colors on each row indicate identical concentration. Hence the "ripples," though strictly artifacts emanating from the truncation, are of only minor importance in typical practical mixing analyses. This demonstrates that the compact method facilitates reliable (qualitative) representation of transient mixing using just a fraction of the eigenmodes.

A quantitative comparison is carried out in terms of the departure $\epsilon_n^* = \max|\boldsymbol{C}_n - \boldsymbol{C}_n^*|$, with $\boldsymbol{C}_n$ and $\boldsymbol{C}_n^*$ the concentrations according to full and compact methods, respectively. Figure 8 gives the corresponding evolution (stars) in contrast with its prediction based on the truncation error ϵ_n in Eq. (9) (circles). This exposes an excellent agreement between the actual and predicted error and thus further substantiates the reliability of estimators (11), which has the important practical implication that approximation errors inherent in utilization of the compact method are *a priori* predictable – and thus controllable. This is demonstrated by the bright and dark areas in Figure 8, which indicate the regimes of applicability of the compact method for tolerances $\epsilon = 10\%$ and $\epsilon = 1\%$, respectively, as predicted by Eq. (11). Moreover, note that the error decays to $\epsilon_n^* \leq 10^{-11}$ for $n \geq n_\epsilon$, with n_ϵ the above lower bounds for the period employed for evaluation of spectrum C_k^0 ($k \leq M$).

The evolution of ϵ_n^* reveals that the compact method introduces substantial errors for earlier parts of the evolution, thus suggesting breakdown of its validity at these stages of the transient. However, this is considerably less dramatic than it may seem. The large departures must, namely, be on grounds of the good qualitative representation of the mixing patterns (Figure 7), primarily attributed to the before-mentioned artificial "ripples" in the concentration field. Hence, they reflect mainly localized effects with an only weak impact on the global mixing behavior.

Performance of a similar analysis for the good-mixing case $T = 1.6$ conveys essentially the same message: reliable prediction of the (developing) mixing patterns by the compact method throughout the entire transient. Figure 9 supports this by way of the evolution over the first 10 periods of the transient for the full method (panel a) and the compact method for $M/N = 10\%$ (panel b), $M/N = 5\%$ (panel c), $M/N = 1\%$ (panel d). Again a good (qualitative) agreement between mixing patterns is attained and departures primarily consists of localized artificial "ripples" in the concentration field reminiscent of those found in the poor-mixing case and more pronounced for lower cut-off M and earlier stages of the progression. The corresponding error ϵ_n^*, given in Figure 10 (stars), together with its prediction (circles) and regimes of applicability of the compact method for tolerances $\epsilon = 10\%$ (bright) and $\epsilon = 1\%$ (dark), further consolidates the good performance of the compact method and the associated estimators. Important to note is that both poor-mixing and good-mixing cases exhibit similar performance for other initial states. This is not elaborated for brevity.

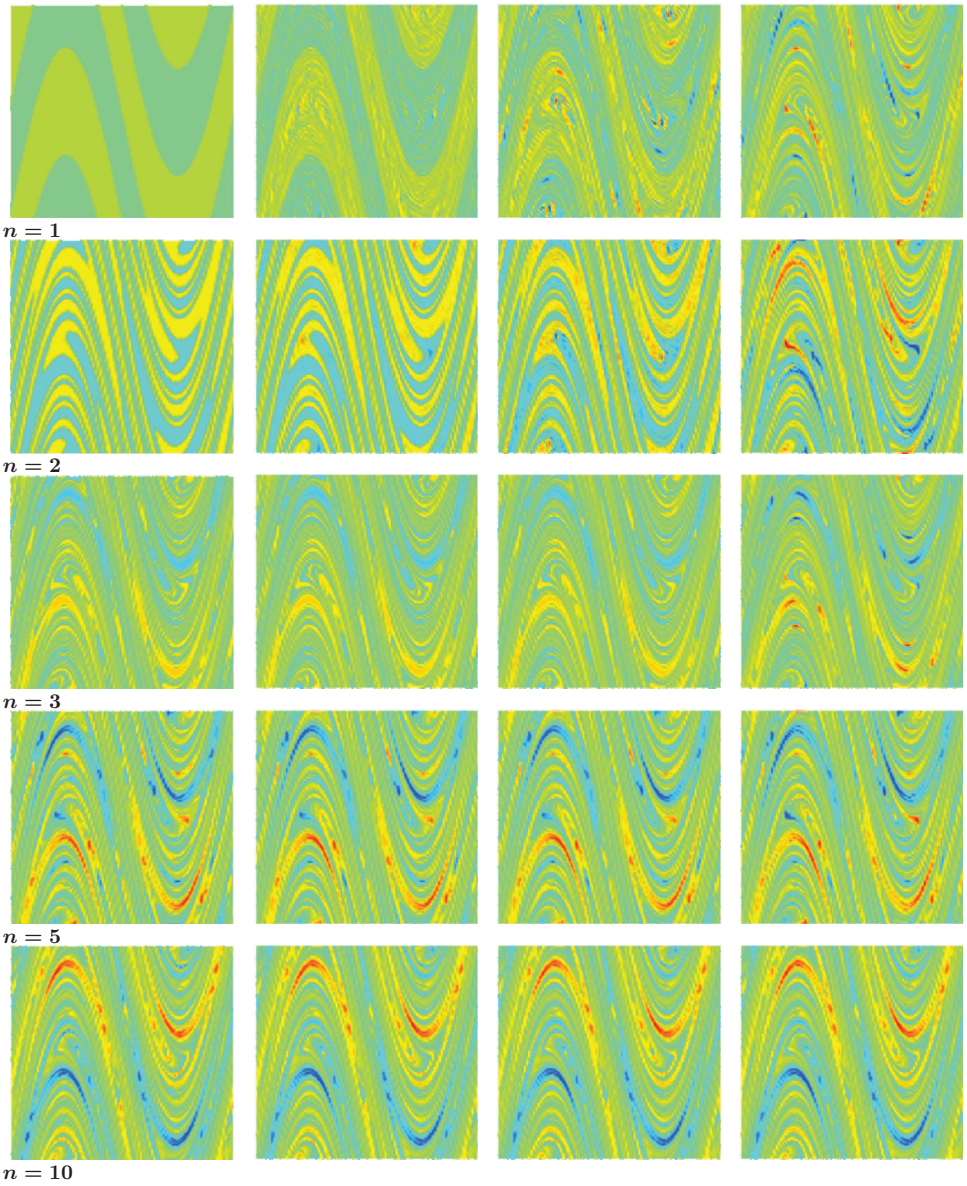

FIG. 9. Evolution starting from initial state I for good-mixing case $T = 1.6$: (a) full mapping method; (b)–(d) compact method for *M*/*N* as indicated. Color coding is adjusted per mapping n (rows) for enhanced contrast; the color blue/red indicates the minimum/maximum for given n.

C. Eigenmode analysis of transient distributive mixing

In Sec. IV B the performance of the compact mapping method was demonstrated. Here, we will investigate *transient* distributive mixing and show that the spectral analysis of compact eigenmodes reveals that concentration transport typically is dominated by limited set of modes: "dominant transient modes." The concept is demonstrated here for the poor-mixing case via the dominant transient modes. To this end the same flow with $T = 0.56$ as studied before is used (where previously the full spectrum and compact spaces *M*/*N* was investigated).

Figure 11 shows the case-specific spectrum C_k^0 for the poor-mixing case $T = 0.56$ and *M*/*N* = 20%. This figure exhibits peaks which thus implies so-called case-specific "dominant transient eigenmodes." Note that the dependence of these dominant eigenmodes on the initial state sets them

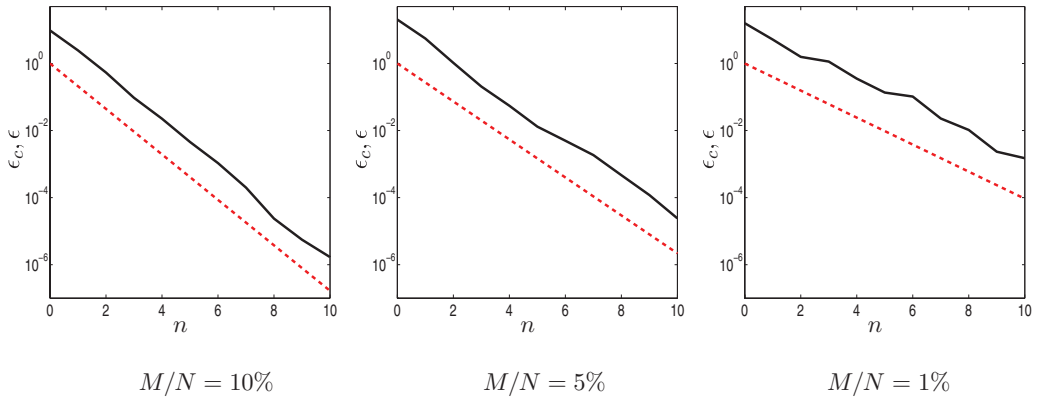

FIG. 10. Departure $\epsilon_c = |\boldsymbol{C}_n - \widetilde{\boldsymbol{C}}_n|$ (solid black line) and its prediction $\epsilon = |\lambda_{M+1}|^n$ dashed line (red) according to Eq. (10) for the good-mixing case $T = 1.6$ and M/N as indicated. Bright and dark areas indicate region of applicability compact method on basis of n following Eq. (11) for $\epsilon = 10\%$ and $\epsilon = 1\%$, respectively.

essentially apart from the dominant eigenmode associated with the asymptotic state. This admits a further reduction of the spectrum via

$$\hat{C}_k^0 = C_k^0 \quad \text{if} \quad |C_k^0| / \max_{k \le M} |C_k^0| \ge C_{\min}, \qquad \hat{C}_k^0 = 0 \quad \text{else} \tag{18}$$

with $C_{\min}$ some preset threshold.

Figure 12 depicts the evolution of mixing patterns for the poor-mixing case $T = 0.56$. Four different cases are compared. The most left column shows the result for the full mapping method and the other three columns for the compact method for M/N as indicated with thresholding following Eq. (18) at $C_{\min} = 10\%$. Concentrations $C < \widehat{C}$ and $C \ge \widehat{C}$ have been set to $C = 0$ and $C = 1$, respectively, with $\widehat{C} = 1/2$ the mean concentration. This creates a pattern of low-concentration (black) and high-concentration (white) regions which is in close agreement with the large-scale mixing patterns. Hence, this mixing pattern is determined by a restricted set of dominant transient eigenmodes. Apparently, the compact mapping method enables the isolation of these eigenmodes and thus offers a way to investigate the underlying fundamental mechanisms. Note that the true mixing pattern must also, for given initial state, strictly consists of black/white patterns in the present context of distributive mixing. The continuous transition from high (red) to low (blue) concentration in Figure 7 is the result of numerical diffusion (colors only in online version).

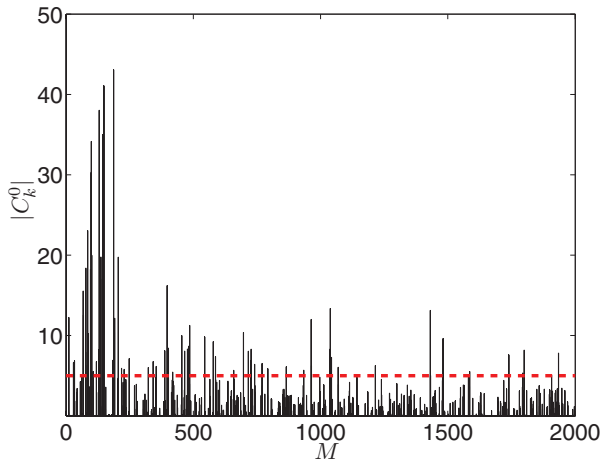

FIG. 11. Case-specific spectrum C_k^0 for the poor-mixing case $T = 0.56$ and $M/N = 20\%$.

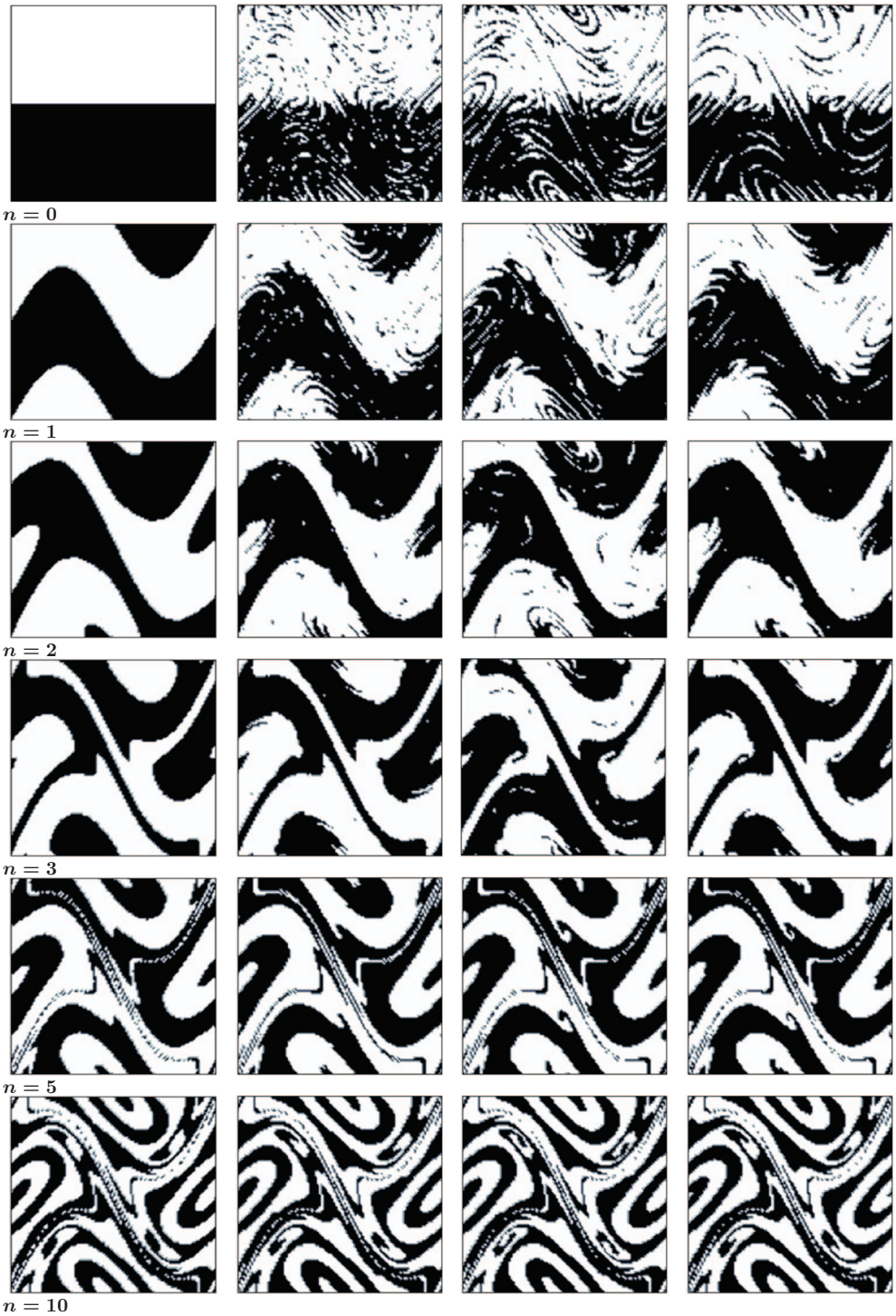

(a) Full mapping (b) $M/N = 20\%$ (c) $M/N = 10\%$ (d) $M/N = 5\%$

FIG. 12. Evolution of mixing patterns for poor-mixing case $T = 0.56$: (a) full mapping method; (b)–(d) compact method for M/N as indicated with thresholding following Eq. (18) at $C_{\min} = 10\%$. Black/white indicate regions with low/high concentrations.

The fact that very small numbers of eigenmodes describe large-scale mixing patterns well suggests that, although this has not been investigated, the compact mapping method may be employed for pattern prediction from experimental data sets of, e.g., geophysical flows.[2,33]

V. CONCLUSIONS

The eigenmode decomposition of the mapping matrix is a powerful approach for the description and explanation of distributive mixing. It deepens understanding of the mixing process and admits investigation of mixing features in terms of physical eigenmodes of the system (approximated by those of the mapping matrix). Spectral analysis thus reveals the Lagrangian structure of the flow field and enables isolation of elliptic islands that deteriorate the quality of the mixing, corresponding with persistent eigenmodes, and chaotic regions and their mixing patterns, determined by dominant eigenmodes. However, for realistic mixing flows the mapping matrix is sparse and very large, rendering a full eigenmode decomposition very expensive and in many cases even impossible. The present study proposes an alternative, more efficient way is required to perform eigenmode analyses in such configurations.

Practical mixing generally involves transient processes that are determined not only by the dominant eigenmode, but also by a limited set of eigenmodes with decay rate significantly lower than the duration of the mixing process. These modes are termed "transient eigenmodes" here and, combined with the dominant eigenmode, defined a compact eigenmode basis that dictates a given mixing flow. This compact basis is substantially smaller than the full eigenmode basis and thus enables a much more efficient eigenmode analysis and, in case of many realistic flows, such an analysis at all. The procedure is as follows. First, systematic isolation of the compact eigenmode basis by way of truncation of the eigenvalue spectrum at a given cut-off based on a preset tolerance. Second, efficient evaluation of the expansion coefficients of the compact representation, which depend essentially on the initial state, via orthogonalization of the compact basis.

Eigenmode analysis of transient mixing with the proposed ansatz facilitates isolation of possible modes, other than the dominant eigenmode, within the compact basis that dominate the transient. Such "dominant transient eigenmodes" may play a role of equal – if not higher – significance than the dominant eigenmode in realistic mixing processes. Fundamental difference with the latter is that the excitation of such transient modes depends essentially on the initial state. Identification of multiple dominant modes may deepen understanding of mixing processes and may also facilitate further reduction of the compact eigenmode basis so as to further enhance computational efficiency.

Investigation of the compact mapping method for a number of representative case studies reveals that it performs well. Reductions of the eigenmode basis by one to two orders of magnitude still enable sufficiently accurate predictions of the mixing characteristics, at least for the envisioned area of application, namely realistic mixing flows. Evolutions predicted by the compact method are in good agreement with reference simulations by the full method. Qualitative agreement is outstanding in that mixing patterns are accurately demarcated for the entire transient. This advances the compact method as a reliable and efficient way for description of (larger-scale features of) transient distributive mixing. The ability to recover such features from, in essence, very limited information suggests that the compact mapping method may be a useful tool in a wider scope for, e.g., pattern prediction from experimental data sets of geophysical or oceanographic flows. Moreover, this implies that mixing processes, even in the early stages of the transient, are typically dominated by a very small – and highly case-specific – set of eigenmodes. Hence, the concept of dominant transient eigenmodes may have great potential for further fundamental studies as well.

[1] S. Wiggins, "The dynamical systems approach to Lagrangian transport in oceanic flows," Annu. Rev. Fluid Mech. **37**, 295 (2005).
[2] A. M. Mancho, D. Small, and S. Wiggins, "A comparison of methods for interpolating chaotic flows from discrete velocity data," Comput. Fluids **35**, 416 (2006).
[3] I. Mezic, S. Loire, V. A. Fonoberov, and P. Hogan, "A new mixing diagnostic and Gulf oil spill movement," Science **330**, 486 (2010).
[4] I. I. Rypina, L. J. Pratt, J. Pullen, J. Levin, and A. L. Gordon, "Chaotic advection in an archipelago," J. Phys. Oceanogr. **40**, 1988 (2010).

[5] R. Mizuta and S. Yoden, "Chaotic mixing and transport barriers in an idealized stratospheric polar vortex," J. Atmos. Sci. **58**, 2616 (2001).
[6] R. T. Pierrehumbert and H. Yang, "Global chaotic mixing on isentropic surfaces," J. Atmos. Sci. **50**, 2462 (1993).
[7] O. V. Popovych, A. Pikovsky, and B. Eckhardt, "Abnormal mixing of passive scalars in chaotic flows," Phys. Rev. E **75**, 036308 (2007).
[8] S. Cerbelli, V. Vitacolonna, A. Adrover, and M. Giona, "Eigenvalue-eigenfunction analysis of infinitely fast reactions and micromixing regimes in regular and chaotic bounded flows," Chem. Eng. Sci. **59**, 2125 (2004).
[9] R. T. Pierrehumbert, "Tracer microstructure in the large-eddy dominated regime," Chaos, Solitons Fractals **4**, 774 (1994).
[10] D. Rothstein, E. Henry, and J. P. Gollub, "Persistent patterns in transient chaotic fluid mixing," Nature (London) **401**, 770 (1999).
[11] G. A. Voth, T. C. Saint, G. Dobler, and J. P. Gollub, "Mixing rates and symmetry breaking in two-dimensional chaotic flow," Phys. Fluids **15**, 2560 (2003).
[12] A. Adrover, S. Cerbelli, and M. Giona, "A spectral approach to reaction/diffusion kinetics in chaotic flows," Comput. Chem. Eng. **26**, 125 (2002).
[13] W. Liu and G. Haller, "Strange eigenmodes and decay of variance in the mixing of diffusive tracers," Physica D **188**, 1 (2004).
[14] D. R. Lester, M. Rudman, G. Metcalfe, and H. M. Blackburn, "Global parametric solutions of scalar transport," J. Comput. Phys. **227**, 3032 (2008).
[15] J. Sukhatme and R. T. Pierrehumbert, "Decay of passive scalars under the action of single scale smooth velocity fields in bounded two-dimensional domains: From non-self-similar probability distribution functions to self-similar eigenmodes," Chaos, Solitons Fractals **66**, 056302 (2002).
[16] M. Giona, S. Cerbelli, and V. Vitacolonna, "Universality and imaginary potentials in advection-diffusion equations in closed flows," J. Fluid Mech. **513**, 221 (2004).
[17] M. K. Singh, M. F. M. Speetjens, and P. D. Anderson, "Eigenmode analysis of scalar transport in distributive mixing," Phys. Fluids **21**, 093601 (2009).
[18] R. Spencer and R. Wiley, "The mixing of very viscous liquids," J. Colloid Sci. **6**, 133 (1951).
[19] P. G. M. Kruijt, O. S. Galaktionov, P. D. Anderson, G. W. M. Peters, and H. E. H. Meijer, "Analyzing mixing in periodic flows by distribution matrices: Mapping method," AIChE J. **47**, 1005 (2001).
[20] T. G. Kang, M. K. Singh, T. H. Kwon, and P. D. Anderson, "Chaotic mixing using periodic and aperiodic sequences of mixing protocols in a micromixer," Microfluid. Nanofluid. **4**, 589 (2008).
[21] M. K. Singh, T. G. Kang, H. E. H. Meijer, and P. D. Anderson, "The mapping method as a toolbox to analyze, design and optimize micromixers," Microfluid. Nanofluid. **5**, 313 (2008).
[22] O. S. Galaktionov, P. D. Anderson, G. W. M. Peters, and H. E. H. Meijer, "Morphology development in Kenics static mixers (application of the extended mapping method)," Can. J. Chem. Eng. **80**, 604 (2002).
[23] O. S. Galaktionov, P. D. Anderson, G. W. M. Peters, and H. E. H. Meijer, "Analysis and optimization of Kenics static mixers," Int. Polym. Process. **18**(2), 138 (2003).
[24] M. K. Singh, O. S. Galaktionov, H. E. H. Meijer, and P. D. Anderson, "A simplified approach to compute distribution matrices for the mapping method," Comput. Chem. Eng. **33**, 1354 (2009).
[25] I. Mezić, "Spectral properties of dynamical systems, model reduction and decompositions," Nonlinear Dyn. **41**, 309 (2005).
[26] C. Rowley, I. Mezić, S. Bagheri, P. Schlatter, and D. Henningson, "Spectral analysis of nonlinear flows," J. Fluid Mech. **641**, 115 (2009).
[27] J. G. Franjione and J. M. Ottino, "Symmetry concepts for the geometric analysis of mixing flows," Philos. Trans. R. Soc. London, Ser. A **338**, 301 (1992).
[28] M. Liu, F. J. Muzzio, and R. L. Peskin, "Quantification of mixing in aperiodic chaotic flows," Chaos, Solitons Fractals **4**, 869 (1994).
[29] J. M. Ottino, *The Kinematics of Mixing: Stretching, Chaos, and Transport* (Cambridge University Press, Cambridge, 1989).
[30] D. S. Watkins, *Fundamentals of Matrix Computations* (Wiley, New York, 2002).
[31] A. R. Gourlay and G. A. Watson, *Computational Methods for Matrix Eigenproblems* (Wiley, London, 1973).
[32] J. H. Wilkinson, *The Algebraic Eigenvalue Problem* (Clarendon, Oxford, 1965).
[33] M. Branicki, A. M. Mancho, and S. Wiggins, "A Lagrangian description of transport associated with a front-eddy interaction: Application to data from the North-Western Mediterranean Sea," Physica D **240**, 282 (2011).